Study on preparation and properties of zinc ferrite and titanium dioxide

Jinlin Yang[1,a], Xingnan HuO[1,b], Zongyu Li[1,c] and Shaojian Ma[1,d]*

College of Resources, Environment and Materials, Guangxi University, Nanning 530004, China

Abstract: In this paper, sulfuric acid leaching high iron zinc calcine was used to prepare and purify zinc ferrite, high temperature roasting method was used to prepare synthetic zinc ferrite, and sol-gel method was used to prepare TiO_2. The properties of the prepared samples ware characterized by XRD, FT-IR, BET, SEM and other methods. The results show that the synthetic zinc ferrite is pure zinc ferrite, and the purified zinc ferrite contains impurities $PbSO_4$. The TiO_2 crystal form prepares at the calcination temperature of 300~550℃ is basically the same, and the crystal form transformation occurs at the calcination temperature of 550~600℃. TiO_2 samples calcines at 400℃ (T400) have higher specific surface area, larger total pore volume and average pore diameter. The crystalline degree of synthetic zinc ferrite is high, the micropores on the crystal surface are closed, and the grains bond with each other. The specific surface area, total pore volume and average pore diameter of purified zinc ferrite are larger than those of synthetic zinc ferrite. The effects of specific surface area, pore volume and pore structure on the adsorption capacity and catalytic efficiency are as follows: T400> purified zinc ferrite > synthesized zinc ferrite.

1. Introduction

Zinc ferrite is a kind of metal oxide with spinel structure, which has stable chemical properties, non-toxic and harmless, no photochemical corrosion effect, excellent electromagnetic characteristics and gas sensitive characteristics, high temperature resistance and corrosion resistance, so it is widely used in many fields[1]. There are two main sources of zinc ferrite: one is the by-product of zinc ferrite produced in the process of refining metallurgy, for example, there are zinc ferrite by-products in the dust of electric arc furnace steelmaking and the leaching residue of traditional zinc hydrometallurgy. The other is synthetic zinc ferrite. There are many methods to synthesize zinc ferrite, among which the common methods mainly include sol-gel method, chemical coprecipitation method, hydrothermal synthesis method and high temperature roasting method[2-5]. TiO_2 is an N-type wide band gap semiconductor material with high oxidation efficiency, non-toxicity, stable chemical properties, strong light stability, environmental friendliness and no secondary pollution, and has been widely used in the environmental field. TiO_2 has three crystal forms, namely anatase, rutile and brookite[6]. According to the morphology of chemical substances in the reaction process, TiO_2 can be prepared by solid phase method, liquid phase method and gas phase method. Due to the excellent physical and chemical properties of zinc ferrite and TiO_2, the research on their adsorption and catalytic degradation of dye wastewater as adsorbents and photocatalysts has been developed rapidly. In this paper, zinc ferrite was purified by sulfuric acid leaching of high iron zinc calcine, zinc ferrite was synthesized by high temperature roasting, and TiO_2 was prepared by sol-gel method. The microstructure and surface morphology of the prepared samples are characterized and analyzed by XRD, FT-IR, BET, SEM, which provide a theoretical basis for the subsequent exploration of the adsorption and catalytic treatment of industrial dye wastewater.

2. Sample preparation

50g of zinc calcine and 350ml of sulfuric acid with a concentration of 120g/L ware added into a beaker. The beaker was placed in a thermostatic water bath at a stirring speed of 400 rpm. After leaching for 120min, the beaker was removed, and the supernatant was removed after standing for cooling, filtered it and washed it until the filtrate was neutral. The filter cake was dried and powdered, and the obtained sample was denoted as PZ.

A certain amount of ZnO and Fe_2O_3 were weighed according to the stoichiometric ratio of $ZnFe_2O_4$, mixed and placed in a grinding tank, the mixture was transferred to a ceramic crucible after mechanical activation for 3h, roasted in a high temperature resistance furnace in the air atmosphere, raised the temperature from 100℃ to 800℃

[a]email: 1915392020@st.gxu.edu.cn, [b]email: 2215394007@st.gxu.edu.cn
[c]email: 2215394012@st.gxu.edu.cn
*Correspondence author: [d]email: 1615391004@alu.gxu.edu.cn

at a rate of 10℃/min, held for 1.5h, removed, cooled and then ground. The obtained samples are denoted as SZ.

TiO_2 precursor was prepared by sol-gel method. Transferred it to a ceramic crucible, roasted it in the air atmosphere of a high temperature resistance furnace, heated it up from 100℃ to the set temperature (300℃, 350℃, 400℃, 450℃, 500℃, 550℃, 600℃) at the rate of 10℃/min, held it for 2h, and then ground it after cooling. The obtained samples were denoted as T300, T350, T400, T450, T500, T550 and T600, respectively.

3. Characterization analysis

3.1 XRD analysis

The X-ray diffraction pattern of purified zinc ferrite and synthetic zinc ferrite are shown in Fig. 1(a). The 2θ diffraction angles of the main diffraction peaks of synthesized zinc ferrite are located at 18.190 °, 29.919 °, 35.264 °, 36.867 °, 48.44 °, 53.110 °, 56.629 ° and 62.212 ° respectively, which correspond to the (111), (220), (311), (222), (400), (422), (511) and (440) crystal planes of zinc ferrite, and there are no other impurity peaks in the spectrum. The synthetic zinc ferrite could be judged as pure zinc ferrite. The impurity peaks are located at 2θ=20.944°, 23.324°, 25.579°, 26.712°, 27.689°, 43.748°, 44.545° in the spectrum of purified zinc ferrite. The impurity could be identified as $PbSO_4$. The semi-quantitative analysis showed that the purified zinc ferrite was composed of 94% zinc ferrite and 6% lead sulfate. It can be seen from the diffraction spectra that the diffraction peaks of synthetic zinc ferrite have large peak intensity, narrow and sharp peak type, indicating that the synthetic zinc ferrite has good crystallinity and large grain size. Compared with synthetic zinc ferrite, the diffraction peak intensity of purified zinc ferrite is weaker and the peak shape is wider, which showed that the crystallinity of purified zinc ferrite was not as good as that of synthetic zinc ferrite, and the grain size was smaller than that of synthetic zinc ferrite. This may be due to the fact that the roasting temperature of zinc concentrate is lower than that of synthetic zinc ferrite, so that the by-product zinc ferrite is also generated at a lower temperature or the roasting time of zinc ferrite synthesis is longer than that of purified zinc ferrite, which promotes the growth of grains.

From Fig. 1(b) that the peak positions of the diffraction peaks of TiO_2 calcined at 300~550 ℃ are basically the same, which indicated that the crystals of TiO_2 calcined at 300~550℃ ware basically the same, but the width and intensity of the diffraction peaks changed with the increase of temperature. The precursor of TiO_2 prepared in the experiment showed a crystal transformation between 550 and 600℃. It was also found in the experiment that TiO_2 calcined at 300℃ and 350℃ was black, while most of TiO_2 calcined at 400℃ was light yellow, and a small part of it was translucent maroon. It may be that the organic matter in the gel is not completely burned due to too low calcination temperature. The diffraction spectrum of the TiO_2 also shows that the peak type of the TiO_2 is wider, and the intensity is weaker under the calcination temperature of 300~400℃. It also showed that the crystallinity of the TiO_2 was lower under the condition of lower calcination temperature. The diffraction spectrum that with the increase of temperature, the peak type of the diffraction peak narrows and the intensity increases, indicating that the crystal form of TiO_2 tended to be complete.

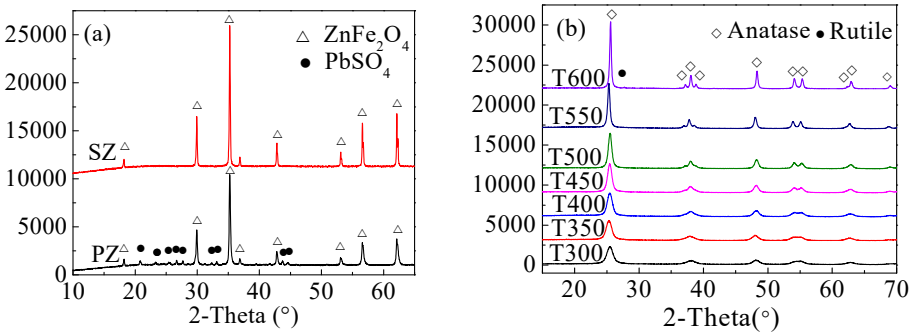

Fig. 1(a) XRD spectra of purified $ZnFe_2O_4$ and synthetic $ZnFe_2O_4$, (b) XRD spectra of TiO_2 with different calcination temperatures

3.2 SEM analysis

Fig. 2 shows the SEM images of various samples prepared.

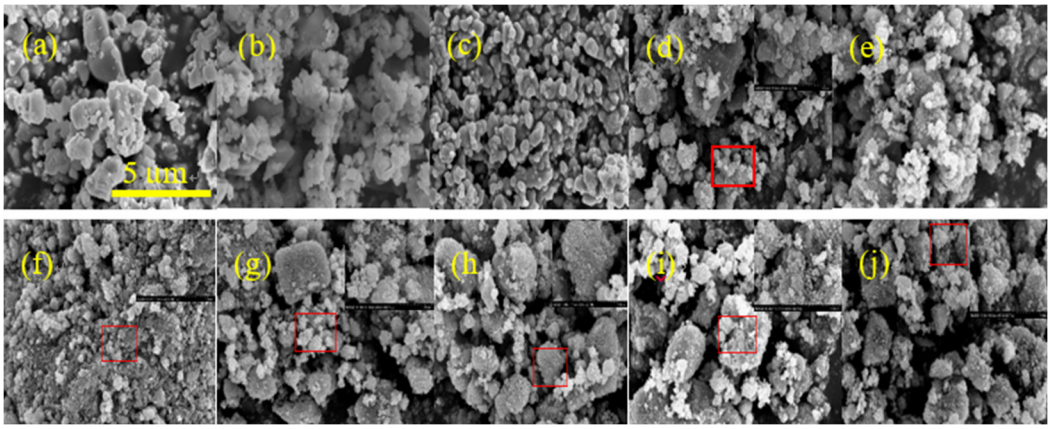

Fig. 2 SEM photographs of (a) Before PZ pulverization; (b) After PZ pulverization;(c) SZ; (d) T300; (e) T350; (f) T400; (g) T450; (h) T500; (i) T550; (j) T600

It can be seen from Fig. 2(a) and Fig. 2(b), the surface of purified zinc ferrite particles is smooth before pulverization, and the fine size content of purified zinc ferrite particles increases after pulverization, and the shape of the particles changes greatly, many of the edges and corners of the particles become more and more sharp, and the agglomeration among the particles is intensified. Fig. 2(c) shows the synthetic zinc ferrite prepared by calcination method. The particle size distribution is uniform, the crystals are well developed and the grains are bonded to each other. Fig. 2(d)~(j) shows TiO_2 calcined at different temperatures. Each sample is broken by vibration mill. Due to insufficient grinding, TiO_2 particles are coarse. From the SEM image, the maximum diameter of particles is about 5μm, the minimum diameter is about 100nm. The particle size distribution is uneven, there are many coarse particles, and the bonding between grains is serious.

3.3 FT-IR analysis

The FT-IR spectra of purified zinc ferrite and synthetic zinc ferrite are shown in Fig.3(a). The FT-IR spectra of TiO_2 calcined at different temperatures are shown in Fig. 3(b). It can be seen from Fig.3(a) that the absorption peaks at 3433cm^{-1} and 1632cm^{-1} of purified zinc ferrite and synthetic zinc ferrite are caused by the stretching vibration and deformation vibration of the water-adsorbed –OH adsorbed water in the sample, and the peaks at 1382cm^{-1} are the KBr interference peak during sample tablet pressing. In the range of 600~400cm^{-1} wave number, there are two very obvious absorption characteristic peaks in the purified zinc ferrite. It is generally believed that this is the characteristic peak of the infrared spectrum of ferrite compound. The absorption peak of 558cm^{-1} belongs to the vibration of Zn–O bond in tetrahedral position, and the absorption peak of 447cm^{-1} belongs to the vibration of Fe–O bond in octahedral position. The synthetic zinc ferrite also shows strong absorption at 558cm^{-1} and 447cm^{-1}. In addition, there is an obvious absorption peak near 1106cm^{-1} for the purified zinc ferrite, which is caused by the antisymmetric stretching vibration of SO_4^{2-}, and it is consistent with the results of XRD analysis.

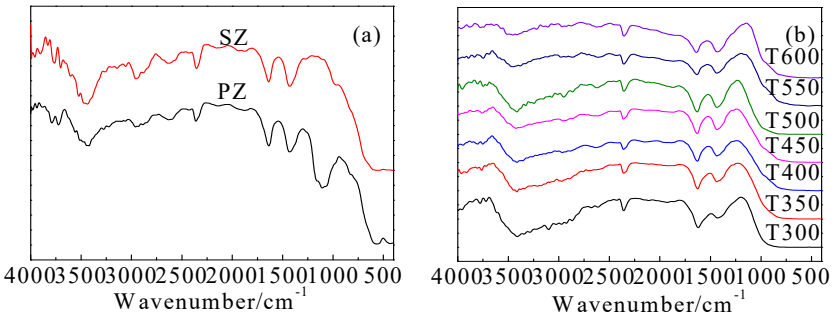

Fig. 3(a) FT-IR spectra of purified $ZnFe_2O_4$ and synthetic $ZnFe_2O_4$, (b) FT-IR spectra of TiO_2 with different calcination temperatures

It can be seen from Fig. 3(b) that the broad and strong absorption peak between 400~800cm^{-1} is the stretching vibration of Ti–O–Ti bond[7], the absorption peak between 1626cm^{-1} and 3000~3600cm^{-1} corresponds to the stretching vibration and bending vibration of O–H of adsorbed water[8]. In the spectrum of the sample T300, there is an obvious absorption peak near the wave number of 3000cm^{-1}, which is caused by the stretching vibration of C–H. In the process of sample preparation, the TiO_2 calcined at this temperature is black, which is due to the low calcination temperature and the incomplete combustion of organic matters in tetrabutyl titanate. There are no other obvious absorption peaks except the stretching vibration absorption peak of Ti–O–Ti bond between 400~800cm^{-1} and the stretching vibration and bending vibration of O–H of adsorbed water between 1626cm^{-1} and 3000~3600cm^{-1}. The calcined sample contains a large amount of –OH, which is caused by the adsorption of water during sample preparation. The absorption peak between 400~800cm^{-1} corresponds to the characteristic absorption peak of TiO_2. It can be seen from Fig. 3 (a) and Fig. 3 (b) that each sample has an absorption peak near 2360cm^{-1}, which is caused by the antisymmetric stretching vibration of CO_2. From the above analysis, it

can be seen that the TiO_2 prepared at each temperature has been basically formed.

3.4 Specific surface areas and pore size analysis

The nitrogen adsorption-desorption curves of purified zinc ferrite, synthetic zinc ferrite and TiO_2 are shown in Fig. 4. The pore size can be divided into: microporous (<2nm), mesoporous (2~50nm) and macropores (>50nm). The pore size distribution of these samples was fitted by BJH model.

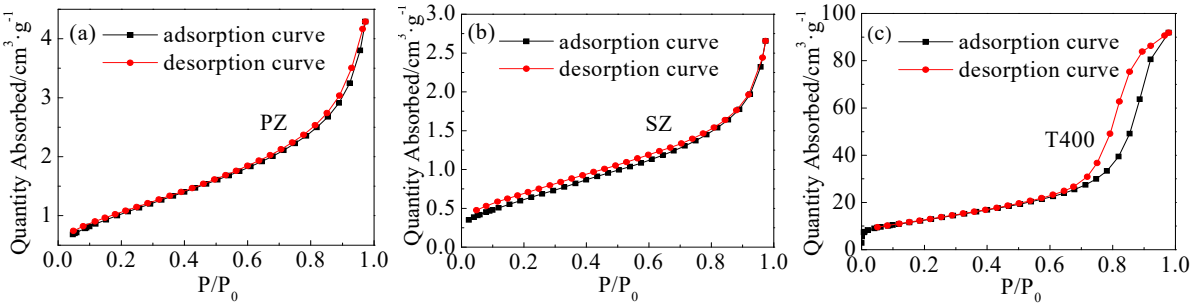

Fig. 4 Adsorption-desorption curves of purified $ZnFe_2O_4$ (a), synthetic $ZnFe_2O_4$ (b) and T400 (c)

It can be seen from Fig. 4(a) and Fig. 4(b) that the adsorption isotherms of them belong to Class III adsorption isotherms and such adsorption isotherms mostly occur on non-porous metal oxides[9]. The adsorption isotherm of purified zinc ferrite shows a slight hysteresis in the high-pressure region, forming a small hysteresis loop, which may be due to the corrosion of sulfuric acid in the leaching process of purified zinc ferrite formed a small number of pores. The amount of N_2 adsorption of the synthetic zinc ferrite is lower than that of the purified zinc ferrite. That showed it had fewer pores. It can be seen from Fig. 4(c) that the adsorption isotherm of T400 belongs to Class IV isotherm, indicating that T400 surface may have mesopores or macropores.

The pore size distribution of purified zinc ferrite, synthetic zinc ferrite and T400 is shown in Fig. 5. The pore size and specific surface area is shown in Table 1.

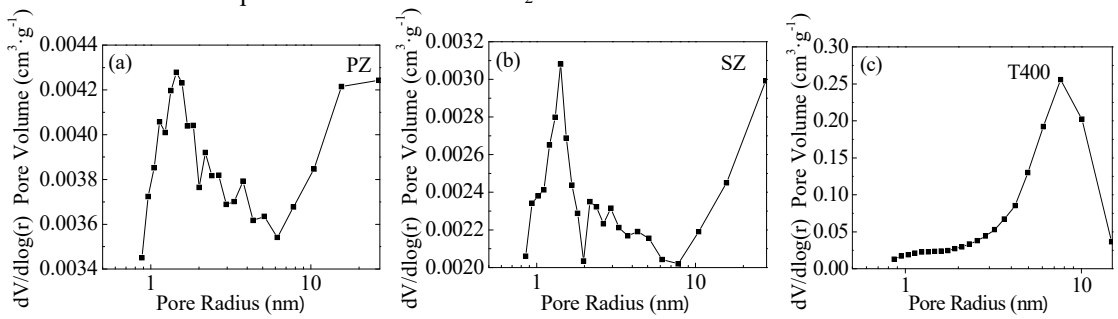

Fig. 5 Adsorption pore volume distribution curves of purified $ZnFe_2O_4$ (a), synthetic $ZnFe_2O_4$ (b) and T400 (c)

Table 1 The pore size and specific surface area of the purified $ZnFe_2O_4$, synthetic $ZnFe_2O_4$ and T400.

Sample	Specific surface area/$m^2 \cdot g^{-1}$	Total pore volume/$cm^3 \cdot g^{-1}$	Average aperture/nm
PZ	3.93	0.0064	5.89
SZ	2.4	0.0039	3.17
T400	45.95	0.1359	5.32

It can be seen from Fig. 5(a) and Fig. 5(b), the pore volume distribution curves of purified zinc ferrite and synthesized zinc ferrite show two most probable peaks, and the most probable pore diameter is about 3nm. The pore size distribution characteristics of the two materials are similar, mainly concentrated in the mesopore range, and the distribution is discontinuous. It can be seen from Fig. 5(c), the volume distribution curve of the adsorption pore of T400 has a most probable peak, and its most probable pore diameter is about 15nm, and the pore diameter is continuously distributed, mainly between 4nm~30nm, belonging to mesopore.

It can be seen from Table 1 that T400 has a higher specific surface area, and the total pore volume and average pore size are larger. The specific surface area, total pore volume and average pore diameter of purified zinc ferrite are larger than those of synthetic zinc ferrite. First, the purified zinc ferrite may have more pore structure due to sulfuric acid erosion during the leaching process, and the particle size of the purified zinc ferrite after pulverization is smaller. Second, it may be due to the high calcination temperature and high degree of crystallization during the preparation of synthetic zinc ferrite, the micropores on the crystal surface are closed, and the grains are bonded to each other, which is consistent with the SEM analysis results.

4 Conclusions

(1)The synthetic zinc ferrite was pure zinc ferrite, and the purified zinc ferrite contained impurity $PbSO_4$, which was composed of 94% zinc ferrite and 6% lead sulfate. When the calcination temperature range was 300~550℃, the crystal forms of TiO_2 under different calcination temperatures ware basically the same. When the calcination temperature was 550~600℃, the crystal form changed and rutile TiO_2 appeared; compared with purified zinc ferrite, the synthetic zinc ferrite had uniform particle size, better crystallinity and larger grain size. When the calcination temperature was low, the degree of crystallization of TiO_2 was low. With the increase of temperature, the crystal form of TiO_2 tended to be complete.

(2)The pore structure of purified zinc ferrite, synthesized zinc ferrite and T400 was mainly mesoporous. T400 has the higher specific surface area and larger total pore volume and average pore diameter. In the preparation process of synthetic zinc ferrite, the calcination temperature was high, the crystallization degree was high, the micropores on the crystal surface ware closed, and the grains ware bonded with each other. Compared with the synthetic zinc ferrite, the purified zinc ferrite has more pore structure due to the corrosion of sulfuric acid during leaching, and the specific surface area, the total pore volume and the average pore diameter of the purified zinc ferrite are larger than those of the synthetic zinc ferrite.

(3)The specific surface area, pore volume and pore structure of purified zinc ferrite, synthetic zinc ferrite and T400 are important parameters affecting their adsorption capacity and catalytic efficiency. The order of the effects of the specific surface area, pore volume and pore structure on the adsorption capacity and catalytic efficiency were as follows: T400> purified zinc ferrite> synthesized zinc ferrite.

Acknowledgements

The authors would like to acknowledge the financial support received from National Natural Science Foundation of China (No. 52264020, No. 51774099).

References

1. Singh N B, Agarwal A. (2018) Preparation, characterization, properties and applications of nano zinc ferrite[J]. Materials Today: Proceedings, 5(3), 9148-9155.
2. Koleva K V, Velinov N I, Tsoncheva T S, et al. (2013) Preparation, structure and catalytic properties of $ZnFe_2O_4$[J]. Bulg. Chem. Commun, 45(4), 40-47.
3. Vinosha P A, Mely L A, Jeronsia J E, et al. (2017) Synthesis and properties of spinel $ZnFe_2O_4$ nanoparticles by facile co-precipitation route[J]. Optik, 134, 99-108.
4. Wang W, Li N, Hong K, et al. (2019) Z-scheme recyclable photocatalysts based on flower-like nickel zinc ferrite nanoparticles/ZnO nanorods: enhanced activity under UV and visible irradiation[J]. Journal of Alloys and Compounds, 777: 1108-1114.
5. Xu M, Yang J L, Ma S J, et al. (2016) Experimental research on preparation of Zinc Ferrite by roasting[J]. Mining and Metallurgical Engineering, 36(3): 74-77.
6. Augustynski J. (1993) The role of the surface intermediates in the photoelectrochemical behaviour of anatase and rutile TiO_2[J]. Electrochimica Acta, 38(1), 43-46.
7. Kasap S, Tel H, Piskin S. (2011) Preparation of TiO_2, nanoparticles by sonochemical method, isotherm, thermodynamic and kinetic studies on the sorption of strontium[J]. Journal of Radioanalytical & Nuclear Chemistry, 289(2), 489-495.
8. Florence Bosc, André Ayral, Pierreantoine Albouy Albouy, et al. (2003) A simple route for low-temperature synthesis of mesoporous and nanocrystalline anatase thin films[J]. Chemistry of Materials, 15(12), 2463-2468.
9. Translated by Li Guoxi. (2005) Science of Adsorption (2nd Edition). Beijing: Chemical Industry Press, 32-35.